VOL. 13, NO. 6, MARCH 2018 ISSN 1819-6608
ARPN Journal of Engineering and Applied Sciences

www.arpnjournals.com

HALL CURRENT AND CHEMICAL REACTION EFFECTS ON FREE CONVECTIVE FLOW PAST AN ACCELERATED MOVING VERTICAL PLATE WITH RAMPED TEMPERATURE: FEM

Siva Reddy Sheri[1], K. Rajeshwar Reddy[2], Anjan Kumar Suram[1] and M. Chenna Krishna Reddy[3]
[1]Department of Mathematics, GITAM University, Hyderabad Campus, Telangana, India
[2]Department of Mathematics, Malla Reddy College of Engineering & Technology, Medchal, Telangana, India
[3]Department of Mathematics, Osmania University, Hyderabad, Telangana, India
E-Mail: sreddy7@yahoo.co.in

ABSTRACT

A numerical investigation has been adopted to study chemical reaction effect on free convective flow past an accelerated moving vertical plate with ramped temperature. The governing equations of flow, heat and mass transfer are solved by employing finite element method. Numerical results for the velocity, temperature and concentration distributions for various parametric values are reported graphically and discussed. The influence of various important parameters on primary skin-friction coefficient, secondary skin-friction coefficient and the Nusselt number are shown in a tabular form. The accuracy of the numerical method is validated by a direct comparison with previously published work and found that there is an excellent agreement between the results exists.

Keywords: free convection, hall current, chemical reaction, ramped temperature, FEM.

INTRODUCTION

The phenomena of free convection arise in the fluid flow when temperature or concentration change causes density variation leading to buoyancy forces acting on the fluid elements. Natural convective flow is prevalent in many natural phenomena and has varied and wide range industrial applications. It plays a vital role in our environment. This can be seen in our everyday life in the atmospheric flow, which is driven by temperature or concentration differences. Natural processes such as vaporization of mist and fog, photosynthesis, drying of porous solids, transpiration, sea-wind formation and formation of ocean currents occur due to thermal and solutal buoyancy forces developed as a result of a difference in temperature or concentration or a combination of these two. Such configurations are also encountered in several practical systems for industry-based applications, viz., heat exchanger devices, cooling of molten metals, insulation systems, petroleum reservoirs, filtrations, chemical catalytic reactors and processes, nuclear waste repositories, desert coolers and wet bulb thermometers. Literature related to free convection flow has been undertaken by several authors. Chandran *et al.* [1] have studied unsteady hydromagnetic free convection flow with heat flux and accelerated boundary motion. Palani and Abbas [2] have investigated free convection MHD flow with thermal radiation from an impulsively started vertical plate. Abdul Gaffer *et al.* [3] have analyzed free convection flow and heat transfer of non-Newtonian tangent hyperbolic fluid from an isothermal sphere with partial slip. Abdul Gaffer *et al.* [4] have performed Computational analysis of magneto hydrodynamic free convection flow and heat transfer of non-Newtonian tangent hyperbolic fluid from a horizontal circular cylinder with partial slip. Nandkeolyar and Das [5] have examined MHD free convective radiative flow past a flat plate with ramped temperature in the presence of inclined magnetic field. Chandra Rajvanshi *et al.* [6] have investigated Effect of radiation and gravity modulation on unsteady MHD free convection flow through porous medium in slip-flow regime with entropy.

The Hall affect creates the voltage difference across an electric conductor, cross ways to the current and perpendicular to the magnetic field. Edwin Herbert Hall discovered this effect in 1879. The characteristics of current in a conductor are responsible for the occurrence of Hall affect. This effect plays a prominent role in differentiating the positive and negative charges moving in opposite directions. Hall affect has proved that the electric current flows in metals by the moving electrons and not by protons. It is also shown by the Hall affect that the current in P-Type semiconductors is due to positive holes moving instead of negative electrons. Hall probes are used as magnetometers to measure magnetic fields or inspect materials by using magnetic flux leakage. Hall effect devices require amplification as they produce very low signals. They are suitable for laboratory instruments. Hall affect devices are resistant to contaminants like dust and water. In recent years many advances are taking place in improvising these devices. Other applications of these sensors include the rotating speed sensors in automobiles, cycles etc., they can be used for sensing fluid flows and can also be used for sensing pressure. Researchers and academicians have advanced their studies relating to problems involving Hall Current are: Satya Narayana *et al.* [7] have studied effects of Hall current and radiation absorption on MHD micro polar fluid in a rotating system. Effects of Hall current, radiation and rotation on natural convection heat and mass transfer flow past a moving vertical plate by Seth *et al.* [8]. Hall effects on an unsteady magneto-convection and radiative heat transfer past a porous plate by Das *et al.* [9].

Combined heat and mass transfer problems with chemical reactions are of importance in many processes. Therefore, they have received a considerable amount of attention in recent years. In the processes such as drying, evaporating at the surface of a water body, transferring energy in a wet cooling tower and flowing in a desert cooler, heat and mass transfer occur simultaneously. Possible applications of this type of flows can be found in many industries. For example, in the power industry, electrical energy is extracted directly from a moving conducting fluid. Many practical diffusive operations involve the molecular diffusion of a species in the presence of a chemical reaction within or at the boundary. There are two types of reactions. One is the homogeneous reaction, which occurs uniformly throughout a given phase. The species generation in a homogeneous reaction is analogous to the internal source of the heat generation. The other is the heterogeneous reaction, which takes place in a restricted region or within the boundary of a phase. It can also be treated as a boundary condition similar to the constant heat flux condition in heat transfer. The study of heat and mass transfer with chemical reactions is of great practical importance to engineers and scientists because of its almost universal occurrence in many branches of science and engineering. The flow of a fluid past a wedge is of fundamental importance since it constitutes a general and wide class of flows in which the free stream velocity is proportional to the power of the length coordinate measured from the stagnation point. Due to this one several authors contributed in this area. Chamkha *et al*. [10] have studied Heat and mass transfer from truncated cones with variable wall temperature and concentration in the presence of chemical reaction effects. Chamkha *et al*. [11] have investigated unsteady heat and mass transfer by MHD mixed convection flow from a rotating vertical cone with chemical reaction and Soret and Dufour Effects. Patil and Pop [12] have analyzed Effects of surface mass transfer on unsteady mixed convection flow over a vertical cone with chemical reaction. Murti *et al*. [13] have reported radiation, chemical reaction, double dispersion effects on heat and mass transfer in non-Newtonian fluids. Venkataramana Reddy *et al*. [14] have studied chemically reacting MHD dusty Nano fluid flow over a vertical cone with non-uniform heat source/sink.

In all these investigations, analytical or numerical solutions are obtained by considering conditions for fluid velocity and temperature at the plate as continuous and well defined. However, there exist several problems of practical interest which may require non-uniform or arbitrary thermal conditions. Keeping in view of this fact Narahari [15] has studied Transient free convection flow between long vertical parallel plates with ramped wall temperature at one boundary in the presence of thermal radiation and constant mass diffusion. Seth *et al.* [16] have investigated Natural convection heat and mass transfer flow with hall current, rotation, radiation and heat absorption past an accelerated moving vertical plate with ramped temperature. Siva Reddy *et al.* [17] have found Transient approach to heat absorption and radiative heat transfer past an impulsively moving plate with ramped temperature. Siva Reddy *et al.* [18] have analyzed Heat and mass transfer effects on MHD natural convection flow past an impulsively moving vertical plate with ramped temperature. Siva Reddy and Anjan Kumar [19] have examined finite element analysis of heat and mass transfer past an impulsively moving vertical plate with ramped temperature. Sheri Siva Reddy *et al*. [20] studied Heat and mass transfer effects on MHD natural convection flow past an infinite inclined plate with ramped temperature. Anand Rao *et al* [21] have investigated Radiation effects on an unsteady MHD vertical porous plate in the presence of homogeneous chemical reaction. Siva Reddy Sheri and Prasanthi Modugula [22] has found thermal-diffusion and diffusion-thermo effects on MHD flow through porous medium past an exponentially accelerated inclined plate with variable temperature. Siva Reddy Sheri and Prashanthi Modugula [23] have studied Heat and mass transfer effects on unsteady MHD flow over an inclined porous plate embedded in porous medium with Soret-Dufour and chemical Reaction. Siva Reddy Sheri *et al* [24] have found Heat and mass transfer effects on MHD natural convection Flow past an infinite inclined plate with ramped temperature

In view of the above discussions, the authors investigate chemical reaction effects on free convective flow past an accelerated moving vertical plate with ramped temperature. The governing equations for momentum, energy and concentration are transformed into no dimensional equations and then solved numerically by employing an efficient method namely, Finite element method. The results are reported graphically for various physical parameters for flow velocity, temperature and concentration distributions. The present results are compared with previously existing results and obtained a very good agreement.

Formulation of the problem

Consider unsteady hydromagnetic free convection flow of an electrically conducting, viscous, incompressible and temperature dependent heat absorbing and optically thin heat radiating fluid past an infinite moving vertical plate embedded in a porous medium taking Hall effects into account. Choose the coordinate system in such a way that x' - axis is along the length of the plate in the upward direction and y'-axis normal to the plane of the plate in the fluid. A uniform transverse magnetic field B_0 is applied in y'- axis. Both the fluid and plate are in rigid body rotation with uniform angular velocity Ω about y'-axis. Initially i.e. at time $t' \le 0$, both the fluid and plate are at rest and at uniform temperature T'_∞. Also species concentration within the fluid is maintained at uniform concentration C'_∞. At time $t' > 0$, plate starts moving with time dependent velocity $U(t')$ in x' direction and temperature of plate is raised or lowered to $T'_\infty + (T'_W - T'_\infty)t'/t_0$ when $t' \le t_0$, and thereafter, i.e.

at $t' > t_0$, plate is maintained at uniform temperature T'_w. Also at time $t' > 0$, species concentration at the surface of the plate is raised to uniform species concentration C'_w and is maintained thereafter. Geometry of the problem is presented in Figure1. Since plate is of infinite extent along x' and z' directions and is electrically non-conducting, all physical quantities depend on y' and t' only. It is assumed that the induced magnetic field produced by fluid motion is negligible in comparison to the applied one. This assumption is valid because magnetic Reynolds number is very small for metallic liquids and partially ionized fluids (Cramer and Pai [25]). Also no external electric field is applied so the effects of polarization of fluid are negligible (Cramer and Pai [25]).

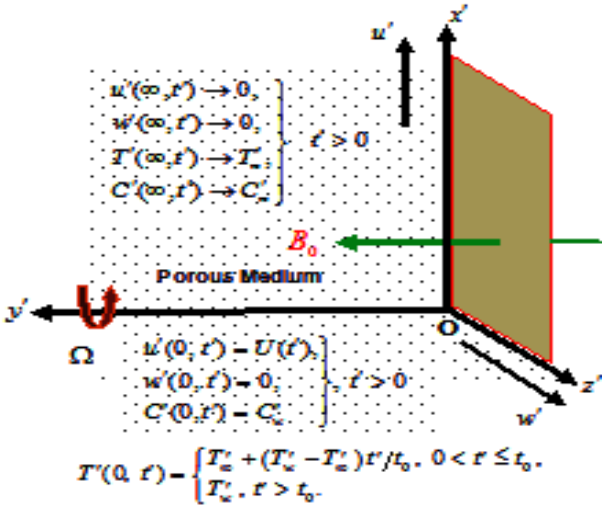

Figure-1. Physical modal of the problem.

Keeping in view of the assumptions made above, the governing equations for unsteady hydro magnetic natural convection flow of a viscous, incompressible, electrically conducting and temperature dependent heat absorbing and optically thin heat radiating fluid in a uniform porous medium taking Hall effects and rotation into account are given by

$$\frac{\partial u'}{\partial t'} + 2\Omega w' = \upsilon \frac{\partial^2 u'}{\partial y'^2} - \left(\frac{\sigma B_0{}^2}{\rho}\right)\frac{(u' + mw')}{(1+m^2)} - \frac{\upsilon}{K_1'}u' + g\beta'(T' - T'_\infty) + g\beta^*(C' - C'_\infty) \quad (1)$$

$$\frac{\partial w'}{\partial t'} - 2\Omega u' = \upsilon \frac{\partial^2 w'}{\partial y'^2} + \left(\frac{\sigma B_0{}^2}{\rho}\right)\frac{(mu' - w')}{(1+m^2)} - \frac{\upsilon}{K_1'}w' \quad (2)$$

$$\frac{\partial T'}{\partial t'} = \frac{k}{\rho c_p}\frac{\partial^2 T'}{\partial y'^2} - \frac{Q_0}{\rho c_p}(T' - T'_\infty) - \frac{1}{\rho c_p}\frac{\partial q'_r}{\partial y'} \quad (3)$$

$$\frac{\partial C'}{\partial t'} = D\frac{\partial^2 C'}{\partial y'^2} - k_r' C' \quad (4)$$

The appropriate initial and boundary conditions for the flow problem are given by

$$u' = w' = 0,\ T' = T'_\infty,\ C' = C'_\infty \ \text{for}\ \ y' \geq 0 \ \text{and}\ t' \leq 0, \quad (5)$$

$$u' = U(t'), w' = 0, C' = C' \ \text{at}\ \ y' = 0 \ \text{for}\ t' > 0, \quad (6)$$

$$T' = T'_\infty + (T'_W - T'_\infty)t'/t_0 \ \text{at}\ \ y' = 0 \ \text{for}\ \ 0 < t' \leq t_0, \quad (7)$$

$$T' = T'_W \ \text{at}\ y' = 0 \quad \text{for}\ t' > t_0, \quad (8)$$

$$u', w' \to 0,\ T' \to T'_\infty,\ \ C' \to C'_\infty \ \text{as}\ \ y' \to \infty \ \ \text{for}\ t' > 0 \quad (9)$$

In the case of an optically thin gray fluid the local radiant absorption (Raptis [26]) is expressed as:

$$\frac{\partial q_r}{\partial y'} = 4a^*\sigma^*(T'^4 - T'^4_\infty) \quad (10)$$

where a^* is absorption coefficient and σ^* is Stefan- Boltzmann constant.

It is assumed that the temperature difference within the fluid flow is sufficiently small such that fluid temperature T'^4 may be expressed as a linear function of the temperature. This is accomplished by expanding T'^4 in a Taylor series about free stream temperature T'_∞. Neglecting second and higher order terms, is expressed as

$$T'^4 \cong 4T'^3_\infty T' - 3T'^4_\infty \quad (11)$$

By using Equations (10) and (11) in Equation (3), we obtain

$$\frac{\partial T'}{\partial t'} = \frac{k}{\rho c_p}\frac{\partial^2 T'}{\partial y'^2} - \frac{16\delta^* T'^3_\infty}{\rho c_p}(T' - T'_\infty) - \frac{Q_0}{\rho c_p}(T' - T'_\infty) \quad (12)$$

Introducing non-dimensional variables and parameters

$$\left.\begin{aligned} &y=\frac{y'}{U_0 t_0}, u=\frac{u'}{t_0}, w=\frac{w'}{t_0}\ t=\frac{t'}{t_0},\ T=\frac{(T'-T'_\infty)}{(T'_w-T'_\infty)},\ C=\frac{(C'-C'_\infty)}{(C'_w-C'_\infty)}, K^2=\frac{\Omega v}{{U_0}^2}, M=\frac{\sigma {B_0}^2 v}{\rho {U_0}^2}, m=\omega_e \tau_e, \\ &K_1=\frac{K'_1 {U_0}^2}{v^2}, Gr=\frac{g\beta' v (T'_w-T'_\infty)}{{U_0}^3} Gc=\frac{g\beta^* v (C'_w-C'_\infty)}{{U_0}^3}, Pr=\frac{vc_p}{k}, R=\frac{16a^* \sigma v {T'_\infty}^3}{{U_0}^2 \rho c_p}, \varphi=\frac{Q_0 v}{\rho c_p {U_0}^2}, \\ &Sc=\frac{v}{D_M} \text{ and } Kr=\frac{k'_r v}{{V_0}^2} \end{aligned}\right\} \quad (13)$$

Making use of equation (13) in Equations (1), (2), (12) and (4) we get non-dimensional form as

$$\frac{\partial u}{\partial t}+2K^2 w=\frac{\partial^2 u}{\partial y^2}-\left(\frac{M}{1+m^2}\right)(u+mw)-\frac{u}{K_1}+GrT+GcC \quad (14)$$

$$\frac{\partial w}{\partial t}-2K^2 u=\frac{\partial^2 w}{\partial y^2}+\left(\frac{M}{1+m^2}\right)(mu-w)-\frac{w}{K_1} \quad (15)$$

$$\frac{\partial T}{\partial t}=\frac{1}{\Pr}\frac{\partial^2 T}{\partial y^2}-RT-\phi T \quad (16)$$

$$\frac{\partial C}{\partial t}=\frac{1}{Sc}\frac{\partial^2 C}{\partial y^2}-KrC \quad (17)$$

It may be noted that characteristic time t_0 may be defined according to the non-dimensional process mentioned above as

$$t_0=\frac{\nu}{{U_0}^2} \quad (18)$$

Where U_0 is characteristic velocity.

Initial and boundary conditions, presented by Equations (5) to (9) in non-dimensional form, are given by

$$u=w=0,\ T=0, C=0 \quad for\ y\geq 0\ and\ t\leq 0, \quad (19)$$

$$u=f(t), w=0,\ C=1\ at\ y=0 \quad for\ t>0, \quad (20)$$

$$T=t\ at\ y=0 \quad for\ 0<t\leq 1, \quad (21)$$

$$T=1\ at\ y=0 \quad for\ t>1, \quad (22)$$

$$u,\ w\to 0\ T\to 0\ C\to 0 \quad as\ y\to\infty \quad for\ t>0 \quad (23)$$

Where $f(t)=U(t')/t_0$

Method of solution

The finite element method is a powerful technique for solving differential or partial differential equations as well as integral equations. The basic concept is that the whole domain is divided into smaller elements of finite dimensions called ‘‘Finite Elements’’. It is the most versatile numerical technique in modern engineering analysis and has been employed to study diverse problems in heat transfer, fluid mechanics, chemical processing, rigid body dynamics, solid mechanics, electrical systems and many other fields. An excellent description of this method is presented in the text books Bathe [27] and Reddy [28]. The finite element method (FEM) consists of following steps

Step 1: Discretization of the domain

The fundamental concept of the FEM is to divide the region of the problem into small connected pieces, called finite elements. The group of elements is called the finite element mesh. These finite elements are associated in a non-overlapping manner, such that they completely cover the entire space of the problem.

Step 2: Invention of the element equations

a) A representative element is selected from the mesh and the variational formulation of the given problem is created over the typical element.

b) Over an element, an approximate solution of the variational problem is invented, and by surrogating this in the system, the element equations are generated.

c) The element matrix, which is also known as stiffness matrix, is erected by using the element interpolation functions.

Step 3: Assembly of the element equations

The algebraic equations so achieved are assembled by imposing the inter element continuity conditions. This yields a large number of mathematical equations known as the global finite element model, which governs the whole domain.

Step 4: Imposition of the boundary conditions

On the accumulated equations, the initial and boundary conditions (19 to 23) are imposed.

Step 5: Solution of assembled equations

The assembled equations so obtained can be solved by any of the numerical methods, namely, Gauss elimination technique, LU decomposition technique, and the final matrix equation can be solved by iterative technique.

Variational formulation

The variational formulation connected with Equations. (14)- (17) Over a typical two-nodded linear element $(y_e,\ y_{e+1})$ is given by

$$\int_{y_e}^{y_{e+1}} w_1\left[\frac{\partial^2 u}{\partial y^2}-\left(\frac{\partial u}{\partial t}\right)-\left(A+\frac{1}{k_1}\right)u-\left(Am+2K^2\right)w+GrT+GcC\right]dy=0 \quad (24)$$

$$\int_{y_e}^{y_{e+1}} w_2\left[\frac{\partial^2 w}{\partial y^2}-\left(\frac{\partial w}{\partial t}\right)-\left(A+\frac{1}{k_1}\right)w-\left(Am+2K^2\right)u\right]dy=0 \quad (25)$$

$$\int_{y_e}^{y_{e+1}} w_3\left[\frac{1}{\Pr}\left(\frac{\partial^2 T}{\partial y^2}\right)-\left(\frac{\partial T}{\partial t}\right)-(R+\phi)T\right]dy=0 \quad (26)$$

$$\int_{y_e}^{y_{e+1}} w_4\left[\frac{1}{Sc}\left(\frac{\partial^2 C}{\partial y^2}\right)-\left(\frac{\partial C}{\partial t}\right)-KrC\right]dy=0 \quad (27)$$

Where $A=\dfrac{M}{(1+m^2)}$ and w_1, w_2, w_3 and w_4 are arbitrary test functions and may be viewed as the variation in u, w, T and C respectively. After dropping the order of integration and non-linearity, we appear at the following system of equations.

$$\int_{y_e}^{y_{e+1}}\left[\left(\frac{\partial w_1}{\partial y}\right)\left(\frac{\partial u}{\partial y}\right)-w_1\left(\frac{\partial u}{\partial t}\right)-\left(A+\frac{1}{k_1}\right)\left(w_1\right)\left(\frac{\partial u}{\partial y}\right)-w\left(Am+2K^2\right)w_1+w_1GrT+w_1GcC\right]dy-\left[\left(w_1\right)\left(\frac{\partial u}{\partial y}\right)\right]_{y_e}^{y_{e+1}}=0 \quad (28)$$

$$\int_{y_e}^{y_{e+1}}\left[\left(\frac{\partial w_2}{\partial y}\right)\left(\frac{\partial w}{\partial y}\right)-w_2\left(\frac{\partial w}{\partial t}\right)-w_2\left(A+\frac{1}{k_1}\right)w-w_2\left(Am+2K^2\right)u\right]dy=0 \quad (29)$$

$$\int_{y_e}^{y_{e+1}}\left[\frac{1}{\Pr}\left(\frac{\partial w_3}{\partial y}\right)\left(\frac{\partial T}{\partial y}\right)-w_3\left(\frac{\partial T}{\partial t}\right)-w_3(R+\phi)T\right]dy=0 \quad (30)$$

$$\int_{y_e}^{y_{e+1}}\left[\frac{1}{Sc}\left(\frac{\partial w_4}{\partial y}\right)\left(\frac{\partial C}{\partial y}\right)-w_4\left(\frac{\partial C}{\partial t}\right)-w_4KrC\right]dy=0 \quad (31)$$

Finite element formulation

The finite element model may be obtained from Equations (28)-(31) by replacing finite element approximations of the form:

$$u=\sum_{j=1}^{4}u_j^e\psi_j^e,\ w=\sum_{j=1}^{4}w_j^e\psi_j^e,\ T=\sum_{j=1}^{4}T_j^e\psi_j^e,$$
$$C=\sum_{j=1}^{4}C_j^e\psi_j^e \quad (32)$$

with $w_1=w_2=w_3=w_4=\psi_j^e$ $(i=1,\ 2,3,4)$,

where u_j^e, $w_{j,}^e$ T_j^e and C_j^e are the primary, secondary velocities, temperature and concentration respectively at the jth node of typical eth element $(y_e,\ y_{e+1})$ and ψ_i^e are the shape functions for this element $(y_e,\ y_{e+1})$ and are taken as:

$$\psi_1^e=\frac{y_{e+1}-y}{y_{e+1}-y_e}\ ,\text{ and }\psi_2^e=\frac{y-y_e}{y_{e+1}-y_e},$$
$$y_e\le y\le y_{e+1} \quad (33)$$

The finite element model of the equations for eth element thus formed is given by

$$\begin{bmatrix} [K^{11}] & [K^{12}] & [K^{13}] & [K^{14}] \\ [K^{21}] & [K^{22}] & [K^{23}] & [K^{24}] \\ [K^{31}] & [K^{32}] & [K^{33}] & [K^{34}] \\ [K^{41}] & [K^{42}] & [K^{43}] & [K^{44}] \end{bmatrix} \begin{bmatrix} \{u^e\} \\ \{w^e\} \\ \{T^e\} \\ \{C^e\} \end{bmatrix} + \begin{bmatrix} [M^{11}] & [M^{12}] & [M^{13}] & [M^{14}] \\ [M^{21}] & [M^{22}] & [M^{23}] & [M^{24}] \\ [M^{31}] & [M^{32}] & [M^{33}] & [M^{34}] \\ [M^{41}] & [M^{42}] & [M^{43}] & [M^{44}] \end{bmatrix} \begin{bmatrix} \{u'^e\} \\ \{w'^e\} \\ \{T'^e\} \\ \{C'^e\} \end{bmatrix} = \begin{bmatrix} \{b^{1e}\} \\ \{b^{2e}\} \\ \{b^{3e}\} \\ \{b^{4e}\} \end{bmatrix} \quad (34)$$

Where $\{[K^{mn}], [M^{mn}]\}$ and $\{\{u^e\}, \{w^e\}\{T^e\}, \{C^e\}, \{u'^e\}, \{w'^e\}\{T'^e\}, \{C'^e\}$ *and* $\{b^{me}\}\}(m, n = 1, 2, 3,4)$

are the set of matrices of order 4×4 and 4×1 respectively. These matrices are defined as follows

$$K_{ij}^{11} = \int_{y_e}^{y_{e+1}} \left[\left(\frac{\partial \psi_i^e}{\partial y} \right) \left(\frac{\partial \psi_i^e}{\partial y} \right) \right] dy,\ M_{ij}^{11} = \int_{y_e}^{y_{e+1}} (\psi_i^e)(\psi_j^e) dy,$$

$$M_{ij}^{12} = M_{ij}^{13} = M_{ij}^{14} = 0,$$

$$K_{ij}^{12} = -\int_{y_e}^{y_{e+1}} \left[\left(A + \frac{1}{k_1} \right) \left(\psi_i^e \right) \left(\frac{\partial \psi_i^e}{\partial y} \right) \right] dy$$

$$K_{ij}^{13} = -\left[\int_{y_e}^{y_{e+1}} \left[\left(\frac{\partial \psi_i^e}{\partial t} \right) \right] dy + \psi_i^e \left(Am + 2K^2 \right) \right] \int_{y_e}^{y_{e+1}} [\psi_i^e] dy,$$

$$K_{ij}^{14} = -[Gr + Gc] \int_{y_e}^{y_{e+1}} (\psi_i^e)(\psi_j^e) dy,$$

$$K_{ij}^{21} = \int_{y_e}^{y_{e+1}} \left[\left(\frac{\partial \psi_i^e}{\partial y} \right) \left(\frac{\partial \psi_i^e}{\partial y} \right) \right] dy,\ M_{ij}^{22} = \int_{y_e}^{y_{e+1}} (\psi_i^e)(\psi_j^e) dy,$$

$$M_{ij}^{21} = M_{ij}^{23} = = M_{ij}^{24} = 0,$$

$$K_{ij}^{22} = -\int_{y_e}^{y_{e+1}} \left[\psi_i^e \left(A + \frac{1}{k_1} \right) \psi_i^e \right] dy,$$

$$K_{ij}^{23} = -\int_{y_e}^{y_{e+1}} \left[(\psi_i^e) \left(\frac{\partial \psi_j^e}{\partial y} \right) \right] dy,$$

$$K_{ij}^{24} = -\int_{y_e}^{y_{e+1}} \psi_j^e \left(Am + 2K^2 \right) \psi_j^e dy$$

$$K_{ij}^{31} = (Ec) \int_{y_e}^{y_{e+1}} \left[(\psi_i^e) \left(\frac{\partial \overline{u}}{\partial y} \right) \left(\frac{\partial \psi_j^e}{\partial y} \right) \right] dy,$$

$$K_{ij}^{32} = -\int_{y_e}^{y_{e+1}} \left[(\psi_i^e) \left(\frac{\partial \psi_j^e}{\partial y} \right) \right] dy + \frac{1}{\Pr} \int_{y_e}^{y_{e+1}} \left[\left(\frac{\partial \psi_i^e}{\partial y} \right) \left(\frac{\partial \psi_j^e}{\partial y} \right) \right] dy,$$

$$K_{ij}^{33} = \frac{1}{\Pr} \int_{y_e}^{y_{e+1}} [\psi_i^e] dy \quad M_{ij}^{33} = \int_{y_e}^{y_{e+1}} (\psi_i^e)(\psi_j^e) dy,$$

$$M_{ij}^{31} = M_{ij}^{32} = M_{ij}^{34} = 0$$

$$K_{ij}^{41} = \int_{y_e}^{y_{e+1}} \left[\frac{1}{Sc} \left(\frac{\partial \psi_i^e}{\partial y} \right) \left(\frac{\partial \psi_i^e}{\partial y} \right) \right] dy,$$

$$K_{ij}^{42} = -\int_{y_e}^{y_{e+1}} \left[\partial \psi_i^e \left(\frac{\partial \partial \psi_i^e}{\partial t} \right) \right] dy,\ K_{ij}^{43} = 0,$$

$$K_{ij}^{44} = \int_{y_e}^{y_{e+1}} [(\psi_i^e) Kr (\psi_i^e)] dy,$$

$$M_{ij}^{44} = \int_{y_e}^{y_{e+1}} (\psi_i^e)(\psi_j^e) dy, M_{ij}^{41} = M_{ij}^{42} = M_{ij}^{43} = 0$$

$$b_i^{1e} = \left[(\psi_i^e) \left(\frac{\partial \psi_j^e}{\partial y} \right) \right]_{y_e}^{y_{e+1}},\ b_i^{2e} = \left[(\psi_i^e) \left(\frac{\partial \psi_j^e}{\partial y} \right) \right]_{y_e}^{y_{e+1}},$$

$$b_i^{3e} = \left[\left(\frac{\psi_i^e}{\Pr} \right) \left(\frac{\partial \psi_j^e}{\partial y} \right) \right]_{y_e}^{y_{e+1}},\ b_i^{4e} = \left[\left(\frac{\psi_i^e}{Sc} \right) \left(\frac{\partial \psi_j^e}{\partial y} \right) \right]_{y_e}^{y_{e+1}}$$

In one-dimensional space, linear and quadratic elements, or element of higher order can be taken. The entire flow region is divided into 1000 quadratic elements of equal size. Each element is three-noded, and therefore the whole domain contains 2101 nodes. At each node, four functions are to be evaluated; hence, after assembly of the element equations, we acquire a system of 8104 equations which are nonlinear. Therefore, an iterative scheme must be developed in the solution. After striking the boundary conditions, a system of equations has been obtained which is solved mathematically by the Gauss elimination method while maintaining a correctness of 0.0001. A convergence criterion based on the relative difference between the present and preceding iterations is employed. When these differences satisfy the desired correctness, the solution is assumed to have been congregated and iterative process is terminated. The Gaussian quadrature is applied for solving the integrations.

Now the expressions for primary skin-friction, secondary skin-friction and Nusselt number are given by

Primary skin-friction coefficient (τ_x) at the plate is given by $\tau_x = \left[\frac{\partial u}{\partial y} \right]_{y=0}$ (35)

Secondary skin-friction coefficient (τ_z) at the plate is given by $\tau_z = \left[\frac{\partial w}{\partial y}\right]_{y=0}$ (36)

The rate of heat transfer coefficient (Nu) at the plate is given by $Nu = \left[\frac{\partial T}{\partial y}\right]_{y=0}$ (37)

Validations of numerical results

In the absence of chemical reaction parameter the present numerical technique has been extensively validated and compared with earlier published work presented by Seth *et al*. [13], and it was found that they are in good agreement, as shown in Tables 1-3.

A comparison of the Primary and secondary skin frictions for ramped temperature and isothermal plate against various values of Schmidt number and time is presented in Tables 1 and 2 respectively. These show that the increase in time tends to enhance primary and secondary skin frictions. Primary skin friction increases and secondary skin friction decreases on increasing values of Schmidt number.

The difference in Nusselt number against thermal radiation, heat absorption and time for ramped and isothermal plates is illustrated in Table-3. It is observed from this table that Nusselt number increases for increasing thermal radiation, heat absorption and time in the case of ramped temperature, where as in the case of isothermal plate Nusselt number decreases with timeand increases with increasing values of thermal radiation and heat absorption.

Table-1. Comparison of skin friction for ramped temperature when $Kr = 0$.

	Seth *et al*. [16]						Present Results					
	$-\tau_x$			τ_z			$-\tau_x$			τ_z		
$Sc \rightarrow$ $t \downarrow$	**0.22**	**0.32**	**0.6**	**0.22**	**0.32**	**0.6**	**0.22**	**0.32**	**0.6**	**0.22**	**0.32**	**0.6**
0.3	0.6431	0.6565	0.6845	0.4775	0.4698	0.4548	0.643099	0.656499	0.68450	0.477500	0.469799	0.454799
0.5	1.3571	1.3673	1.3889	0.7458	0.7398	0.7275	1.357100	1.367299	1.388899	0.745799	0.739800	0.727498
0.7	2.0754	2.0860	2.1043	1.0092	1.0030	0.9925	2.075400	2.086000	2.104299	1.009200	1.003000	0.992499

Table-2. Comparison of skin friction for isothermal plate when $Kr = 0$.

	Seth *et al*. [16]						Present Results					
	$-\tau_x$			τ_z			$-\tau_x$			τ_z		
$Sc \rightarrow$ $t \downarrow$	**0.22**	**0.32**	**0.6**	**0.22**	**0.32**	**0.6**	**0.22**	**0.32**	**0.6**	**0.22**	**0.32**	**0.6**
0.3	0.1890	0.2024	0.2304	0.5664	0.5587	0.5437	0.189000	0.202400	0.230400	0.566399	0.558699	0.543699
0.5	1.0250	1.0351	1.0570	0.8173	0.8113	0.7990	1.024999	1.035100	1.057000	0.817299	0.811299	0.799000
0.7	1.8709	1.8814	1.8998	1.0582	1.052	1.0415	1.870900	1.881399	1.899799	1.058200	1.05200	1.041499

Table-3. Comparison of Nusselt number when $Kr = 0$.

			Seth *et al*. [16]		Present Results	
R	ϕ	t	**Ramped**	**Isothermal**	**Ramped**	**Isothermal**
2	3	0.3	0.88457	1.92093	0.884569	1.920930
2	3	0.5	1.15702	1.89157	1.157020	1.891569
2	5	0.5	1.28383	2.23148	1.283829	2.231479
6	3	0.5	1.40804	2.23148	1.408039	2.231479

RESULTS AND DISCUSSIONS

Extensive numerical computations have been performed with the validated finite element method. In order to verify the accuracy of the numerical method, we have compared our numerical results with that of Seth *et al*. [16]. The comparisons are found to be an excellent agreement. Selected computations have been conducted to study the influence of permeability parameter K_1, rotation parameter K^2, Hall current parameter m, magnetic parameter M, thermal Grashof number Gr, solutal Grashof number Gc, thermal radiation R, heat absorption

parameter ϕ, Prandtl number Pr, Schmidt number Sc and chemical reaction parameter Kr for both ramped and isothermal plates and are presented graphically in Figures 2-28. All data are provided in the legends of these figures correspond to $K^2 = 2.0, M = 15.0, K_1 = 0.2, Gr = 4.0, Gc = 3.0, Pr = 0.71, R = 2.0, \phi = 3.0, Sc = 0.6, Kr = 0.1 and\ t = 0.5.$

Figures 2-3 depict the variations in primary and secondary velocities against various values of permeability parameter for both ramped temperature and isothermal plates. Increasing the porosity of the porous medium clearly serves to enhance the primary and secondary velocities i.e. accelerate the fluid flow. An increased porosity clearly corresponds to a reduced resistance of medium in the flow regime which, therefore, provides a lower resistance to the flow and in turn, boosts the momentum.

Figures 4 and 5 illustrate the influence of rotation parameter on primary and secondary velocities for both ramped and isothermal plate. It is evident from these figures that rotation parameter retards primary velocity and enhances secondary velocity. This due to the reason that rotation tends to slow down the primary fluid velocity whereas it has a reverse effect on secondary fluid velocity for both ramped temperature and isothermal plates which is in agreement with the characteristics of Coriolis force which tends to suppress the primary flow for inducing the secondary flow.

An effect of Hall current parameter on primary and secondary velocities for both ramped and isothermal plates is exhibited in Figures 6-7. A potential proportional to the current and to the magnetic field is developed across the material in a direction perpendicular to both the current and to the magnetic field is called Hall Effect. Increase in the Hall parameter leads to an increase in the primary and secondary velocities. The Hall parameter increases with the magnetic field strength. Physically, the trajectories of electrons are curved by the Lorentz force. When the Hall parameter is low, their motion between the two encounters with heavy particles (neutral or ion) is almost linear. But if it is high, the electron movements are highly curved. Also, because effective conductivity decreases with an increase in Hall parameter which reduces magnetic damping force hence the increase in primary and secondary velocities.

The variation in primary and secondary velocities against magnetic parameter for both ramped temperature and isothermal plates is displayed in Figures 8 and 9. It is obvious that the effect of increasing values of the magnetic parameter M results a decreasing both the velocity distributions across the boundary layer. This is due to the fact that the effect of a transverse magnetic field gives rise to a resistive type force called the Lorentz force. The force has the tendency to slow the motion of the fluid velocities.
The control of thermal Grashof number on primary and secondary velocities for both ramped temperature and isothermal plates is displayed in Figures 10-11. The thermal Grashof number signifies the relative ratio of thermal buoyancy force to the viscous force. Increase in thermal Grashof numbers indicates smaller viscous effect than thermal buoyancy effects in the momentum equations and consequently, causes an increase in the fluid primary and secondary velocities for both ramped temperature and isothermal plates.

Figures 12 and 13 demonstrate the effect of solutal Grashof number Gc on the primary and secondary fluid velocities for both ramped and isothermal plates respectively. It is noticed from these figures that both primary and secondary velocities increase on increasing solutal Grashof number. Gc represents the relative strength of the solutal buoyancy force to the viscous force, Gc increases on increasing the strength of the solutal buoyancy force. This implies that the solutal buoyancy force tends to accelerate the fluid flow in both the primary and secondary flow directions throughout the boundary layer region.

The deviation in primary, secondary velocities and temperature distributions for both ramped and isothermal plates against thermal radiation is illustrated in Figures14- 16. The radiation parameter defines the relative contribution of conduction heat transfer to thermal radiation transfer. Increase in the radiation parameter used to decrease the fluid velocity due to the fact that the momentum boundary layer thickness decreases for increasing the thermal radiation parameter. Increase in radiation parameter leads to decrease the rate of energy transport to the fluid and thereby decreasing the temperature of the fluid. This decrease in the fluid temperature causes the fluid velocities to decrease due to the reduced buoyancy effect.

Figures 17-19 reveal the effect of the heat absorption coefficient on the velocity and temperature for both ramped and isothermal plates. From these figures it is perceived that primary, secondary velocities and temperatures decrease on increasing ϕ. Since heat absorption (thermal sink) has the tendency to reduce the fluid temperature. This causes the thermal buoyancy effects to decrease resulting in a net reduction in the fluid velocity. These behaviors are clearly obvious from Figures17-19 in which primary, secondary velocities and temperature distributions decrease as heat absorption increases. It is also observed that both the hydrodynamic (velocity) and the thermal (temperature) boundary layers decrease as the heat absorption effects increase.

Figures 20-22 elucidate effects of the Prandtl number on momentum and heat transfer for both ramped and isothermal plates. Prandtl number signifies the ratio of momentum diffusivity to thermal diffusivity. It also expresses the ratio of the product of specific heat capacity and dynamic viscosity to the fluid thermal conductivity. It can be noticed from Figures 20 and 21 that the fluid velocities decrease with increasing Prandtl number. Since Prandtl number causes an increase in the viscosity of the fluid which makes the fluid thick and it leads to a decrease in the velocities. It is identified from Figure22 that temperature profile decreases with increasing values of Pr .The reason is that for higher values of Pr, heat is able to diffuse far away from the heated surface more rapidly and thermal boundary layer is thicker for smaller values of Pr ,so the thickness of the thermal boundary layer increases

as Prandtl number decreases and hence temperature profile decreases with increase in Prandtl number.

Figures 23-25 clarify the influence of Schmidt number on the primary, secondary velocities and concentration profiles for both ramped temperature and isothermal plates. Schmidt number is a measure of relative strength of viscosity to chemical molecular diffusivity. From Figures 23 -24 it is understood that Schmidt number retards velocity profiles. It happens due to the reason that mass diffusion tends to decelerate the fluid velocity. Figure25 portrays that concentration profile decreases on increasing Schmidt number .This happens due to the fact that the heavier diffusing species have a greater retarding effect on the concentration distribution of the flow field.

The variation in primary, secondary velocities and concentration against chemical reaction parameter for both ramped temperature and isothermal plates is displayed in Figures 26-28. From Figures 26 and 27 it is identified that chemical reaction parameter tends to decelerate primary and secondary velocities. Since chemical reaction parameter has a of retarding influence on the solute concentration which makes a decrease in the fluid velocity due to reduced mass buoyancy force. It is also noticed from Figure-28 that concentration profile diminishes on increasing chemical reaction parameter. This is due to the reason that chemical reaction parameter has a retarding influence on the concentration distribution of the flow field.

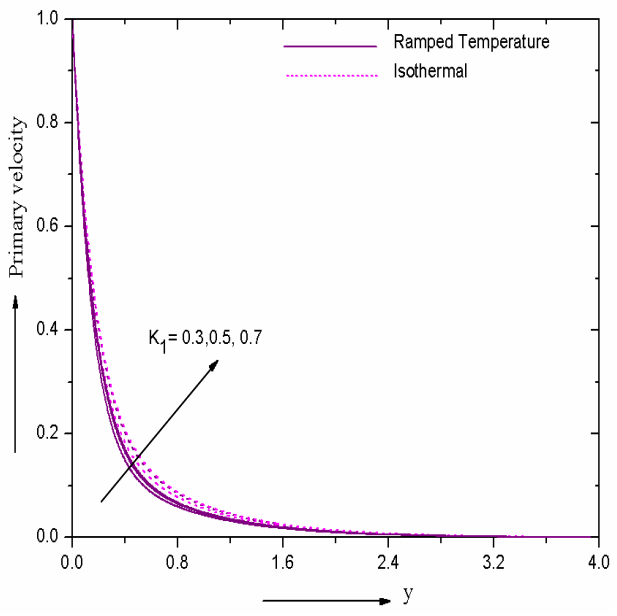

Figure-2. Influence of K_1 on primary velocity.

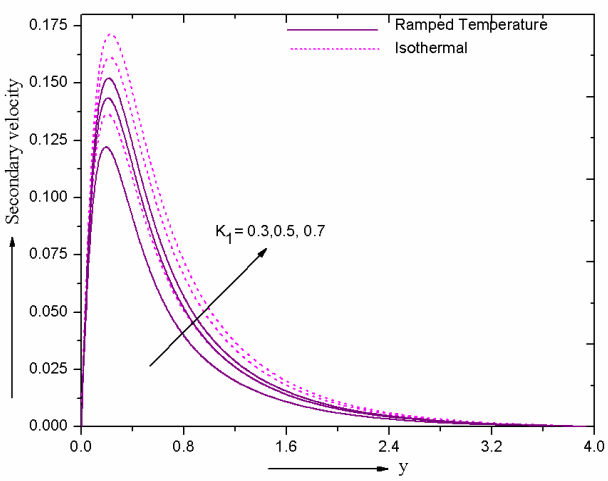

Figure-3. Influence of K_1 on secondary velocity.

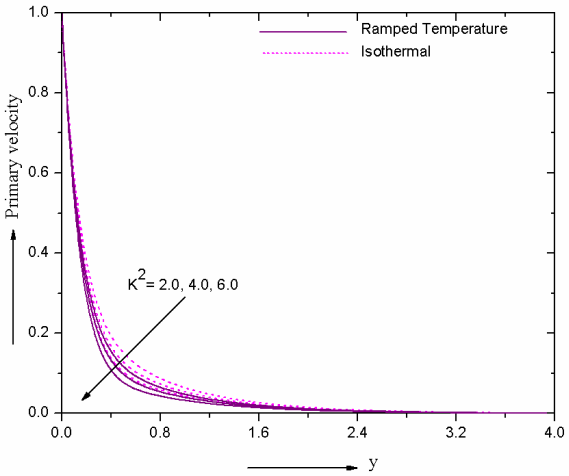

Figure-4. Influence of K^2 on primary velocity.

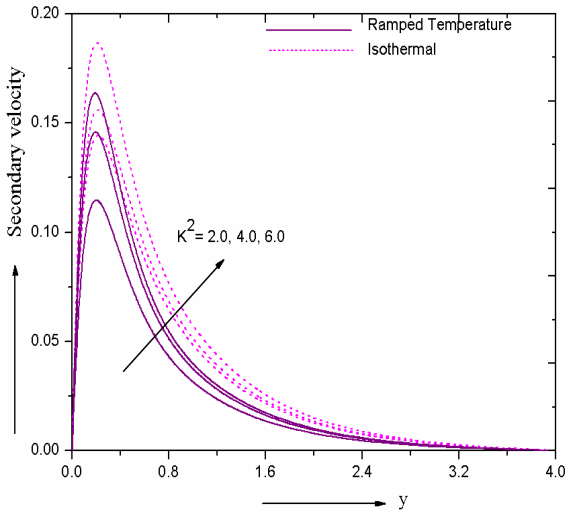

Figure-5. Influence of K^2 on secondary velocity.

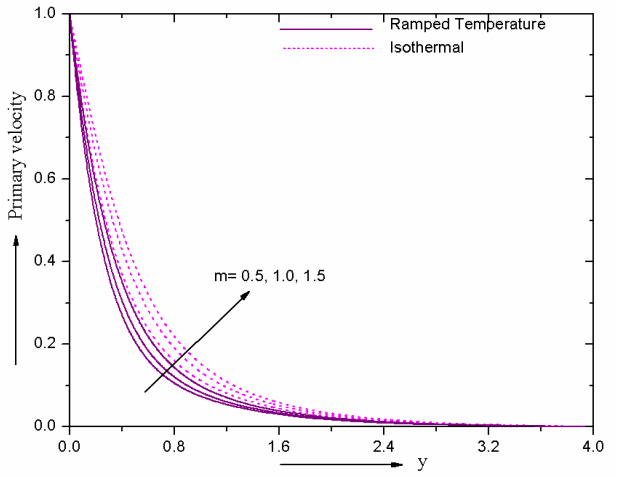

Figure-6. Influence of m on primary velocity.

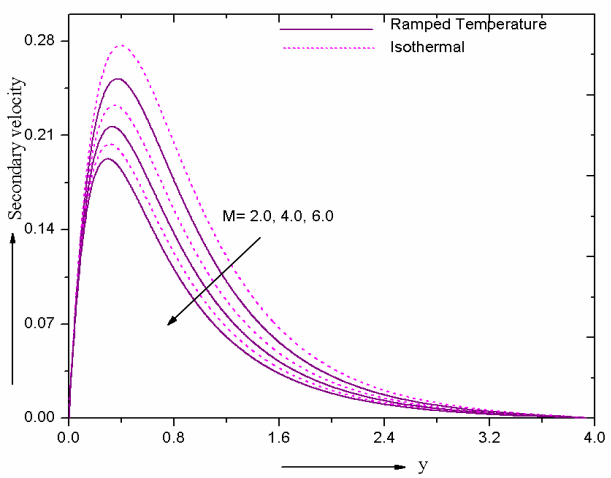

Figure-9. Influence of M on secondary velocity.

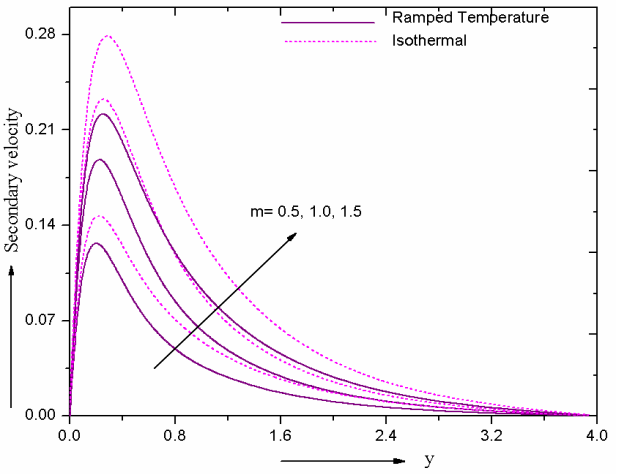

Figure-7. Influence of m on secondary velocity.

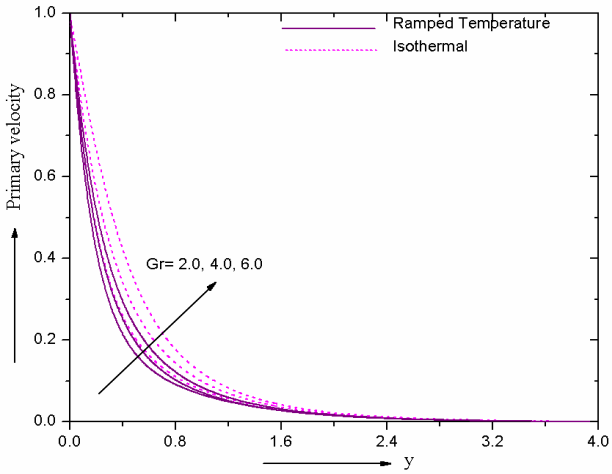

Figure-10. Influence of Gr on primary velocity.

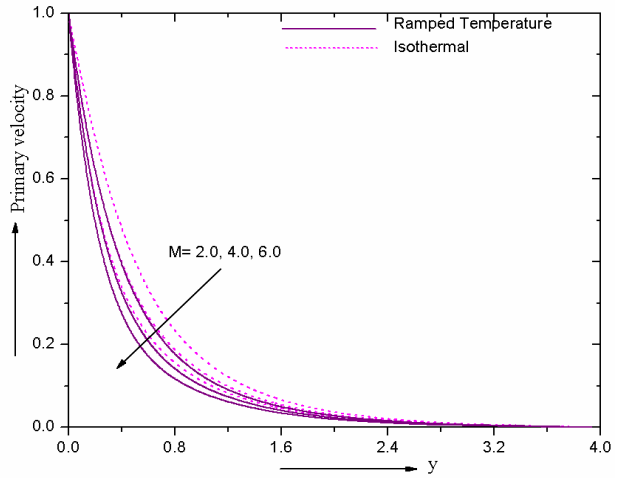

Figure-8. Influence of M on primary velocity.

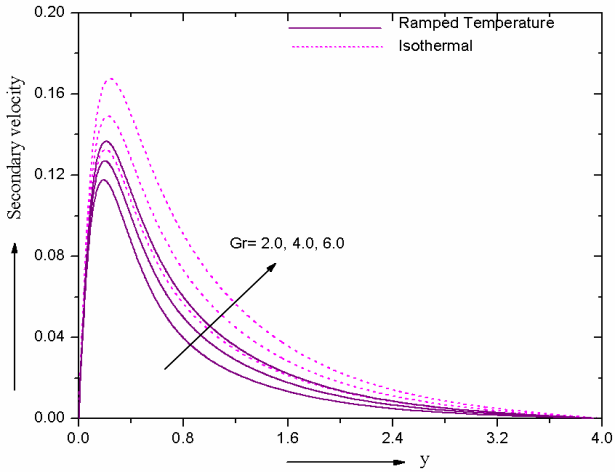

Figure-11. Influence of Gr on secondary velocity.

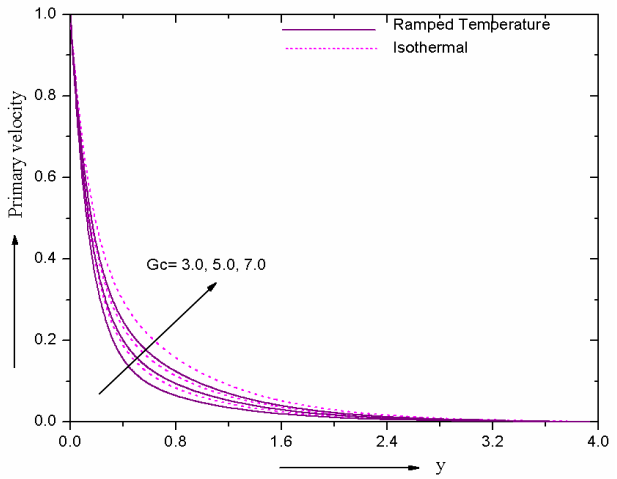

Figure-12. Influence of *Gc* on primary velocity.

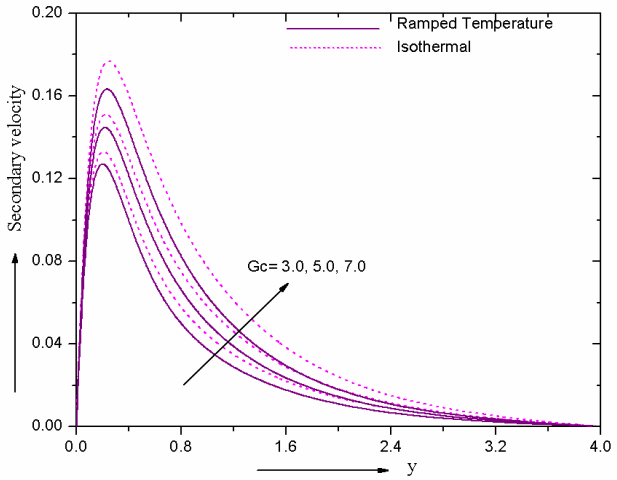

Figure-13. Influenceof *Gc* on secondary velocity.

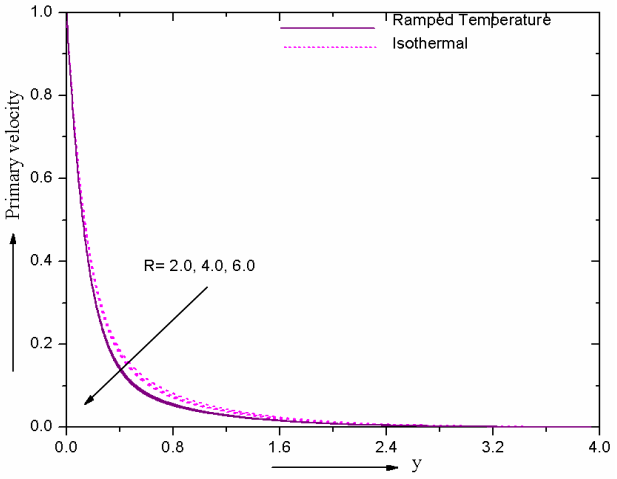

Figure-14. Influence of R on primary velocity.

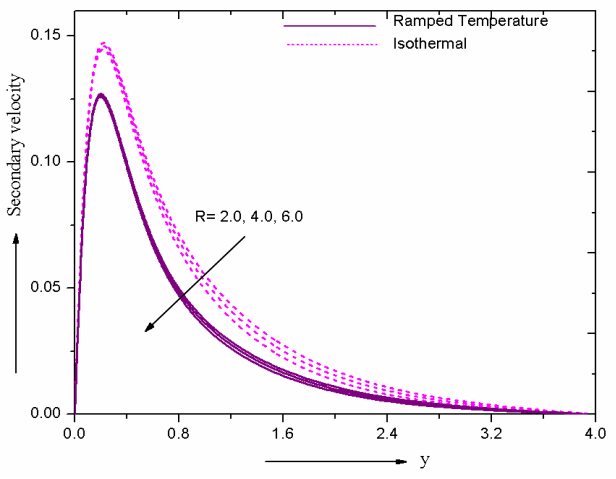

Figure-15. Influence of R on secondary velocity.

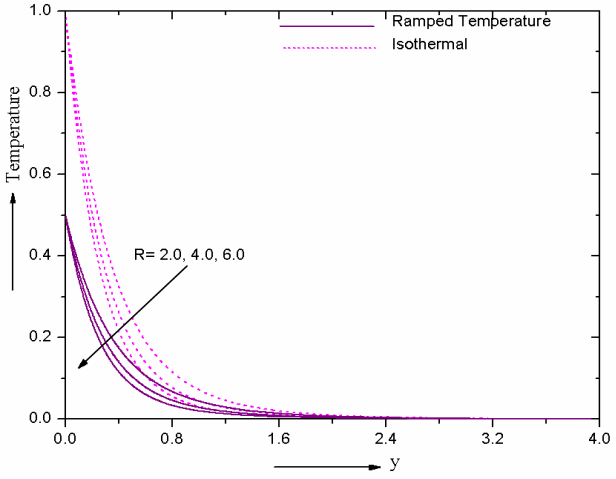

Figure-16. Influence of R on temperature.

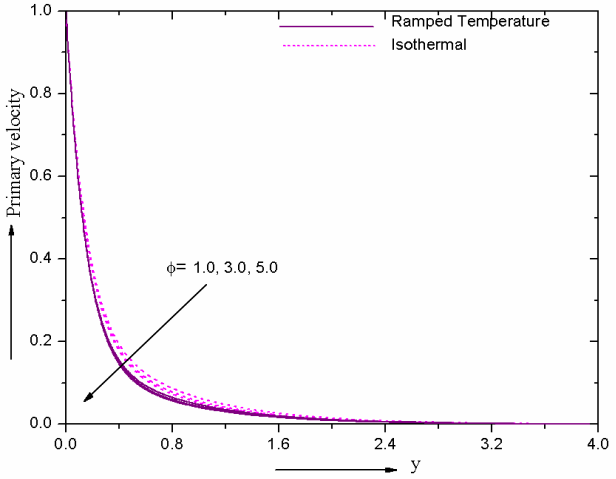

Figure-17. Influence of ϕ on primary velocity.

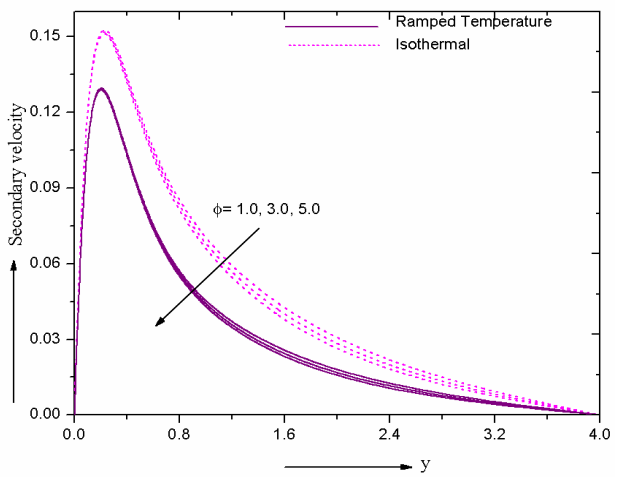

Figure-18. Influence of ϕ on secondary velocity.

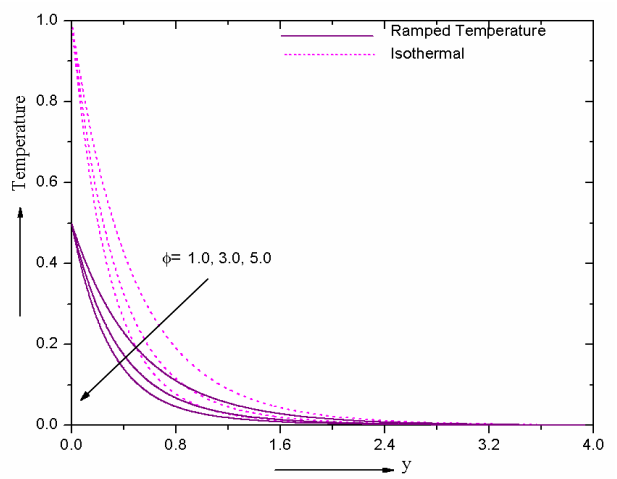

Figure-19. Influence of ϕ on temperature.

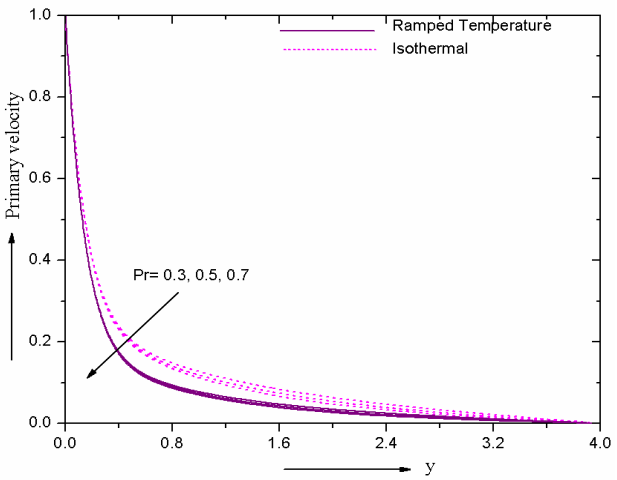

Figure-20. Influence of Pr on primary velocity.

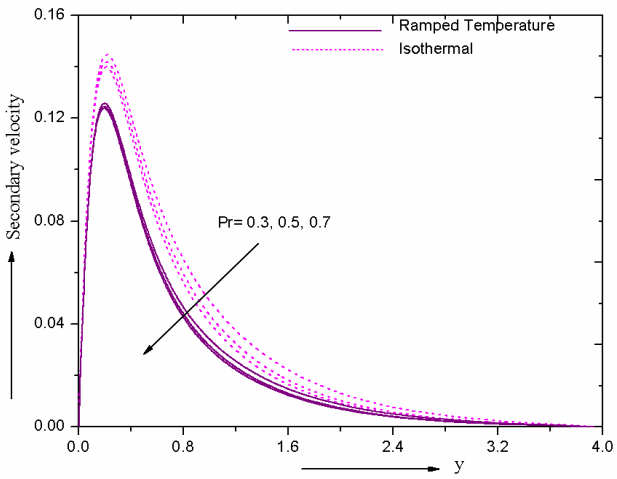

Figure-21. Influence of Pr on secondary velocity.

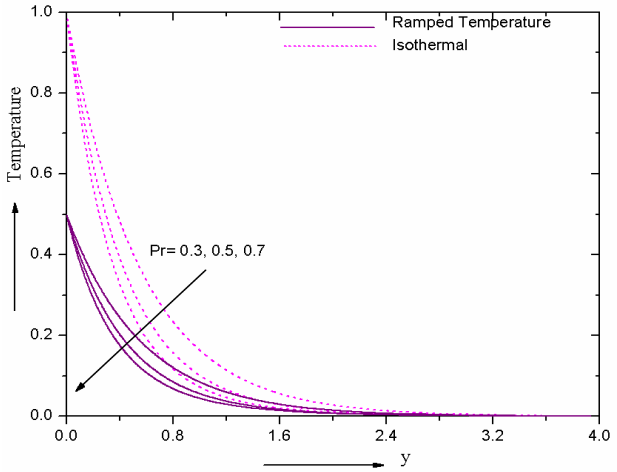

Figure-22. Influence of Pr on temperature.

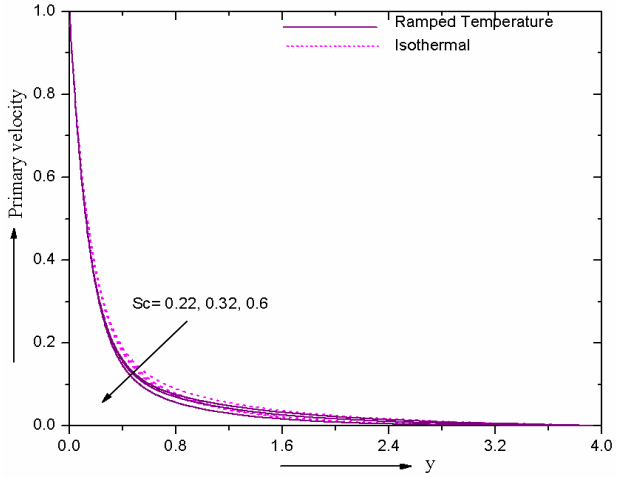

Figure-23. Influence of *Sc* on primary velocity.

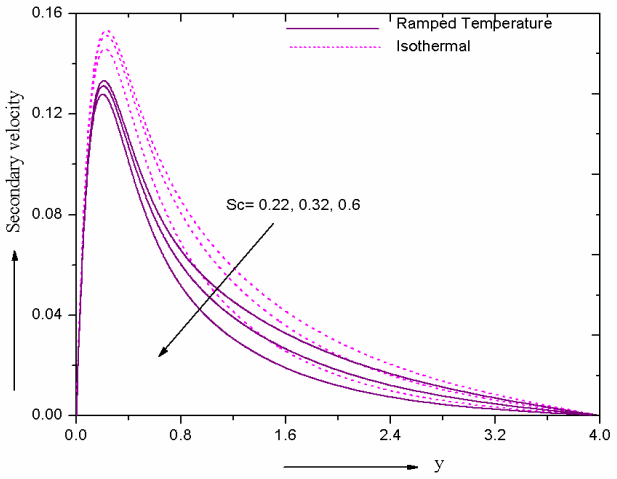

Figure-24. Influenceof *Sc* on secondary velocity.

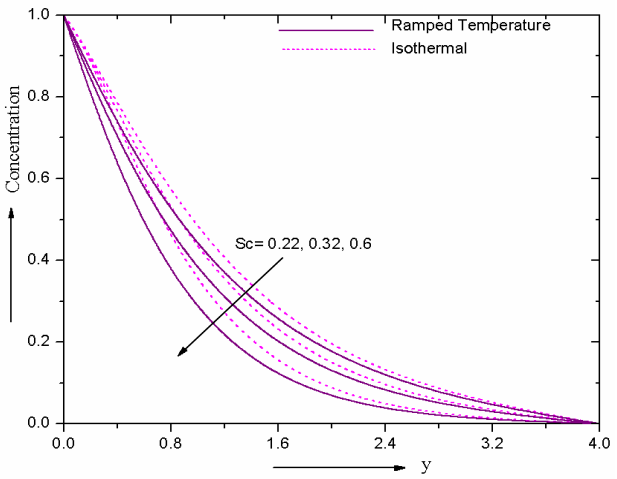

Figure-25. Influence of *Sc* on concentration.

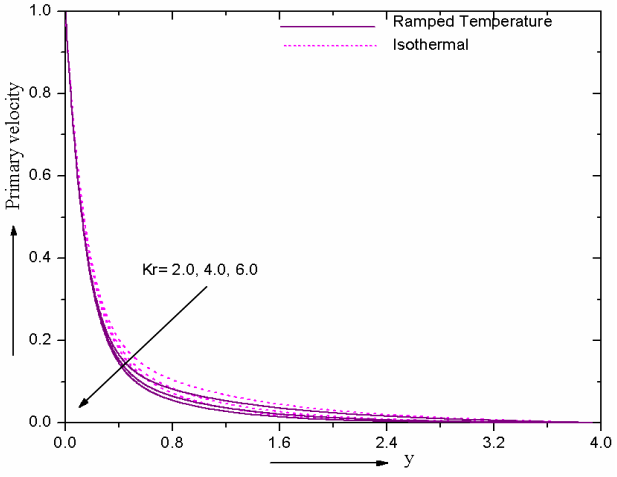

Figure-26. Influence of *Kr* on primary velocity.

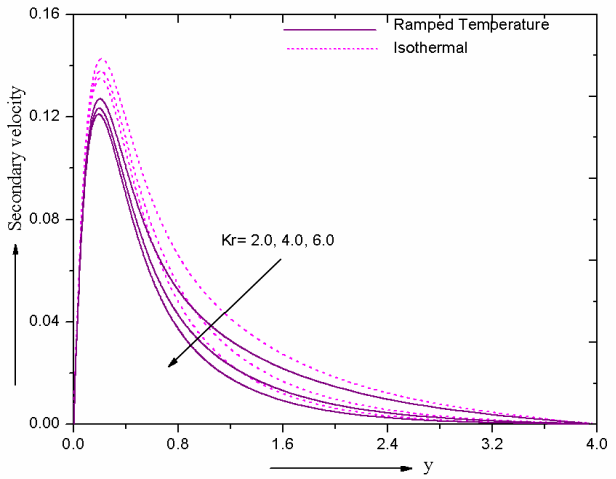

Figure-27. Influence of *Kr* on secondary velocity.

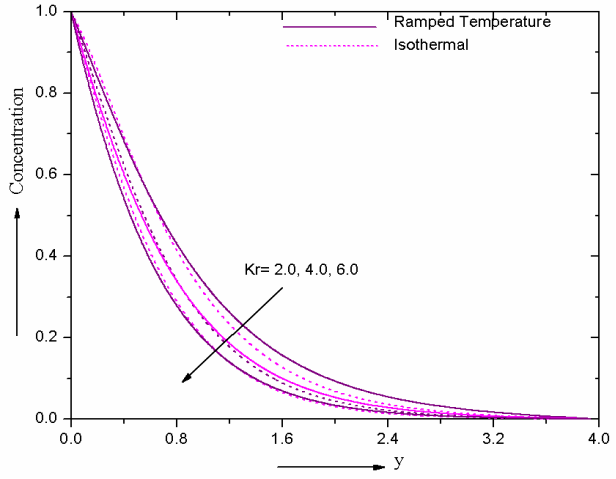

Figure-28. Influence of *Kr* on concentration.

CONCLUSIONS

The influence of chemical reaction on natural convective flow past an accelerated moving vertical plate with ramped temperature has been investigated numerically by using Finite element method. The main conclusions of the present investigations are as follows:

a) Hall current parameter, thermal Grashof number, solutal Grashof number and permeability parameter enhance Primary velocity and magnetic parameter, rotation parameter, Prandtl number, thermal Radiation parameter, heat absorption, Schmidt number and chemical reaction parameter decelerate Primary velocity.

b) Hall current parameter, thermal Grashof number, solutal Grashof number, permeability parameter and rotation parameter tend to increase. But magnetic parameter, Prandtl number, thermal Radiation parameter, heat absorption, Schmidt number and chemical reaction parameter cause to decrease Secondary velocity

c) Increase in Prandtl number, thermal Radiation parameter and heat absorption result a decrease in Temperature profile.
d) Schmidt number and chemical reaction parameter decrease Concentration profile.

REFERENCES

[1] Chandran P, NC Sacheti and AK Singh. 1998. Unsteady hydromagnetic free convection flow with heat flux and accelerated boundary motion. Journal of the Physical Society of Japan. 67: 124- 129, DOI:10.1143/JPSJ.67.124.

[2] G Palani and IA Abbas. 2009. Free convection MHD flow with thermal radiation from an impulsively started vertical plate. Nonlinear Analysis: Modelling and Control. 14: 73-84.

[3] Abdul gaffer, SV Ramachandra Prasad, E Keshava Reddy and O Anwar Beg. 2014. Free convection flow and heat transfer of non-Newtonian tangent hyperbolic fluid from an isothermal sphere with partial slip. Arabian Journal for Science and Engineering. 39: 8157-8174.

[4] Abdulgaffer, SV Ramachandra Prasad and O Anwar Beg. 2015. Computation alanalysis of magneto hydro dynamic free convection flow and heat transfer of non-newtonian tangent hyperbolic fluid from ahorizontal circular cylinder with partial slip. International Journal of Applied and Computational Mathematics. 1: 651-675, DOI: 10.1007/s40819-015-0042-x.

[5] R Nandkeolyar andM Das. 2015. MHD free convective radiative flow past a flat plate with ramped temperature in the presence of inclined magnetic field. Computational and Applied Mathematics. 34:109-123. DOI: 10.1007/s40314-013-0107-6.

[6] Satish Chandra Rajvanshi, Baljinder Singh Saini and Bhawan Jeet. 2014. Effect of radiation and gravity modulation on unsteady MHD free convection flow through porous medium in slip-flow regime with entropy. Walailak Journal of Science and Technology. 11: 225-142.

[7] PV Satya Narayana, B Venkateswarlu and S Venkataramana. 2013. Hall current and radiation absorption on MHD micro polar fluid in a rotating system. Ain Shams Engineering Journal. 4: 843-854.

[8] GS Seth, S Sarkar and SM Hussain. 2014. Effects of Hall current, radiation and rotation on natural convection heat and mass transfer flow past a moving vertical plate. Ain Shams Engineering Journal. 5: 489-503.

[9] S Das, SK Guchait, RN Rana and O Makinde. 2016. Hall effects on an unsteady magneto-convection and radiative heat transfer past a porous plate. Alexandria Engineering Journal. 55: 1321-1331.

[10] AJ Chamkha AM Rashad and H Al-Mudhaf. 2012. Heat and mass transfer from truncated cones with variable wall temperature and concentration in the presence of chemical reaction effects. International Journal of Numerical Methods for Heat and Fluid Flow. 22: 357-376.

[11] AJ Chamkha and AM Rashad. 2014. Unsteady heat and mass transfer by MHD mixed convection flow from a rotating vertical cone with chemical reaction and Soret and Dufour Effects. Can. J. Chem. Eng. 92: 758-767.

[12] PM Patiland IPop. 2011. Effects of surface mass transfer on unsteady mixed convection flow over a vertical cone with chemical reaction. International Journal of Heat Mass Transfer. 47: 1453-1464.

[13] ASN Murti, PK Kameswaran and T Poorna Kantha. 2010. Radiation, chemical reaction, doubles dispersion effects on heat and mass transfer in non-Newtonian fluids. International Journal of Engineering (IJE). 4: 13-25.

[14] Janke Venkata ramana Reddy, Vanagala sugunamma, Naramgari Sandeep and Chakravarthula sk raju. 2017. Chemically reacting MHD dusty Nano fluid flow over a vertical cone with non-uniform heat source/sink. Walailak Journal of Science and Technology. 14: 141-156.

[15] M Narahari. 2012. Transient free convection flow between long vertical parallel plates with ramped wall temperature at one boundary in the presence of thermal radiation and constant mass diffusion. Meccanica. 47: 1961-1976, DOI: 10.1007/s11012-012-9567-9.

[16] GS Seth, R Sharma and S Sarkar. 2015. Natural convection heat and mass transfer flow with hall current, rotation, radiation and heat absorption past an accelerated moving vertical plate with ramped

temperature. Journal of Applied Fluid Mechanics. 8: 7-20.

[17] Sheri Siva Reddy, RS Raju and S Anjankumar. 2015. Transient approach to heat absorption and radiative heat transfer past an impulsively moving plate with ramped temperature. Procedia Engineering. 127: 893-900. DOI: 10.1016/j.proeng.2015.11.427.

[18] Sheri Siva Reddy, Ali J Chamkha and Suram Anjan Kumar.2016.Heat and mass transfer effects on MHD natural convection flow past an impulsively moving vertical plate with ramped temperature. American Journal of Heat and Mass Transfer. 3: 129-148. DOI:10.7726/ajhmt.2016.1009.

[19] Sheri Siva Reddy and Suram Anjan Kumar. 2016. Finite element analysis of heat and mass transfer past an impulsively moving vertical plate with ramped temperature. Journal of Applied Science and Engineering. 19: 385-392. DOI: 10.6180/jase.2016.19.4.01.

[20] Sheri Siva Reddy, Suram Anjan Kumar and Modulgua. Prasanthi. 2016. Heat and mass transfer effects on MHD natural convection flow past an infinite inclined plate with ramped temperature. Journal of the Korean Society for Industrial and Applied Mathematics. 20: 355-374.DOI:10.12941/jksiam.2016.20.355

[21] J. Anand Rao, S. Sivaiah and Sk. Nuslin. 2012. Radiation effects on an unsteady MHD vertical porous plate in the presence of homogeneous chemical reaction. ARPN Journal of Engineering and Applied Sciences. 7: 853-859.

[22] Siva Reddy Sheri and Prasanthi Modugula. 2017. Thermal-diffusion and diffusion-thermo effects on MHD flow through porous medium past an exponentially accelerated inclined plate with variable temperature. ARPN Journal of Engineering and Applied Sciences. 12: 5518-5526.

[23] Siva Reddy Sheri and Prashanthi Modugula. 2017. Heat and mass transfer effects on unsteady MHD flow over an inclined porous plate embedded in porous medium with Soret-Dufour and chemical Reaction. International Journal of Applied and Computational Mathematics. 3: 1289-1306.

[24] Siva Reddy Sheri, Anjan Kumar Suram and Prashanthi Modugula.2016. Heat and mass transfer effects on MHD natural convection Flow past an infinite inclined plate with ramped temperature. Journal of the Korean Society for Industrial and Applied Mathematics. 20: 355-374.

[25] KR Cramer and SI Pai. 1973. Magneto fluid dynamics for Engineers and Applied physicists, McGraw Hill Book Company, NY.

[26] A Raptis. 2011. Free convective oscillatory flow and mass transfer past a porous plate in the presence of radiation for an optically thin fluid. Thermal Science. 15: 849-857.DOI: 10.2298/TSCI101208032R.

[27] KJ Bathe. 1996. Finite Element Procedures, Prentice-Hall, New Jersey.

[28] JN Reddy. 2006. An Introduction to the Finite Element Method, 3rd Edition, McGraw-Hill Book Company, New York.